


Experimental Study of Heat Transfer Parameters of Impingement Heating System Represented by Conductive Target Plate of Resistive film

Dr. Assim H. Yousif

Machines and Equipment Engineering Department, University of Technology/ Baghdad
Email: Assim_yousif2000@yahoo.com

Dr. Amer M. Al Dabagh 

Machines and Equipment Engineering Department, University of Technology/ Baghdad
Email: aamermajeed@yahoo.com

Salah H. Abid Aun

Institute of Technology/ Baghdad

Received on:8/2/2015 & Accepted on:21/4/2016

ABSTRACT:

The current experimental study focuses on the heat transfer characteristics and pressure losses for impingement system which is used in cooling the liner of gas turbine combustor. Recent experiment method of conductive heat transfer technique with resistive film in the back side target plate is introduced. The present experimental model measured both the heat transfer coefficient for inner target surface and the wall cooling effectiveness for outer target surface. To physically explain the phenomena associated with interaction flow area, a computational fluid dynamic code (Fluent 14) is employed. The continuity, momentum and energy equations are computationally solved to analyze the flow field in the jet impingement area. The tests models of the impingement plate are made from round jet holes of inline and staggered arrays arrangement with jet to jet spacing of four-hole diameter. Jet Reynolds numbers of 4200 to 15000 and jet height to diameter ratio of 1.5, 2.0, and 3.0 are maintained. The inline array, as expected enhanced the wall cooling effectiveness over that of the staggered array by 10.3% and both jet spacing and Reynolds number have an evident effect on the discharge coefficient. Empirical correlations are obtained for both arrays arrangement to predict the area-averaged Nusselt number as a function of jet governing parameters.

Keywords: Jet impingement, Cooling effectiveness, Discharge coefficient, Nusselt number.

Nomenclature

A = Target plate surface area, m^2

A_h = Hole cross-sectional area, m^2

G = Secondary mass flow rate per unit frontal surface area, $kg/s.m^2$

C_D = Discharge coefficient.

C_p = Specific heat at constant pressure, $J/kg.K$

D = Jet hole diameter, m

H = Jet to target spacing, m

\bar{h} = Area-averaged heat transfer coefficient, $W/m^2.K$

1588

<https://doi.org/10.30684/etj.34.8A.10>

2412-0758/University of Technology-Iraq, Baghdad, Iraq

This is an open access article under the CC BY 4.0 license <http://creativecommons.org/licenses/by/4.0>

K = Thermal conductivity of the target plate, W/m.K
 L = Length of jet hole, m
 \dot{m} = Mass flow rate, kg/s
 Nu = Nusselt number
 \overline{Nu} = Area-averaged Nusselt number
 P = Jet to jet pitching, m
 Pr = Prandtl number
 Q = Heat flow rate, Watt
 Re = Reynolds number
 S = Jet to jet spacing, m
 s = Second
 t = Time, s
 T = Temperature, degree centigrade
 T_w = Wall temperature, degree centigrade
 X = Local length of the target plate, m
 Z = Thickness of the target plate, m
 η = Wall cooling effectiveness
 $\overline{\eta}$ = Average wall cooling effectiveness
 η_{sa} = Spanwise average wall cooling effectiveness
 ΔP = Change in pressure, N/m²
 ρ = Density of the air, kg/m³

Subscript

$av.$ = average
 $Conv.$ = convection heat transfer
 $Cond.$ = conduction heat transfer
 in = inner target surface
 j = jet
 L = Losses
 o, out = outer target surface
 s = secondary flow
 ∞ = mainstream flow

INTRODUCTION:

Several studies in the past dealt with combustor liner jet impingement cooling were focused on cooling performance and related discharge coefficient. Most studies on impingement cooling in the literature have been conducted to investigate the affecting factors on thermal and aerodynamic performance of impingement cooling system.

Tawfek [1] detected that Nu decreases as the impingement incidence angle becomes smaller than 90° (the normal direction). Zuckerman and Lior [2] showed that for jets spaced at pitch (S) to diameter (D) ratio of jets in an array (S/D) < 4, the adjusted jets are significantly interacted each other. San and Lai [3] showed that for jet height (H) to diameter (D) ratio ($H/D = 2$), the interference persisted up to $S/D = 8$ or 10, and the maximal Nu occurred at $S/D = 8$. Tests modeled on the geometry of the impinging jet devices were done by Changmin et al. [4], Brevet et al. [5], Lamyaa and Deborah [6], Uysal et al. [7], Eric [8] and Lee and Lee [9]. They concluded that the orifice nozzle produces higher heat transfer rate than a fully developed pipe, and using of multiple nozzles to cover a target surface offers some improvements in efficiency and

uniformity of transfer properties. Zuckerman and Lior [10] stated that for a typical single-round impinging jet, the Nu values can vary by a factor of 4 or 5 from radial position to nozzle diameter of 0 to 9. The incorporation of a nozzle array can reduce this variation to a factor of 2. Perapong and Chayut [11] investigated experimentally and numerically two arrays arrangements of jets, inline and staggered at a constant injection distance and hole to hole spacing. Yoshisaburo et al. [12], Jalal et al. [13] and Assim et al. [14] clarified experimentally and numerically the heat transfer characteristics with multiple jets impingement.

Most previous studies concerned with the adiabatic model deal with the inner surface of the target as a test surface, therefore the present work deals with the impingement cooling system performance by using a conductive heat transfer model; such model offers a measuring data that leads to evaluate the effect of impinging jet on the target wall cooling effectiveness.

Experimental Set-up and Procedures

The present test rig consists of two open loops, mainstream and secondary flow lines as shown in Figure (1). In the test section, the philosophy in both cooling and heating wall effectiveness evaluation concept is the same; the wall target plate is heated instead of cooling to save energy. Therefore, the impingement jets from plenum are heated, and the main flow stream is regarded as the coolant.

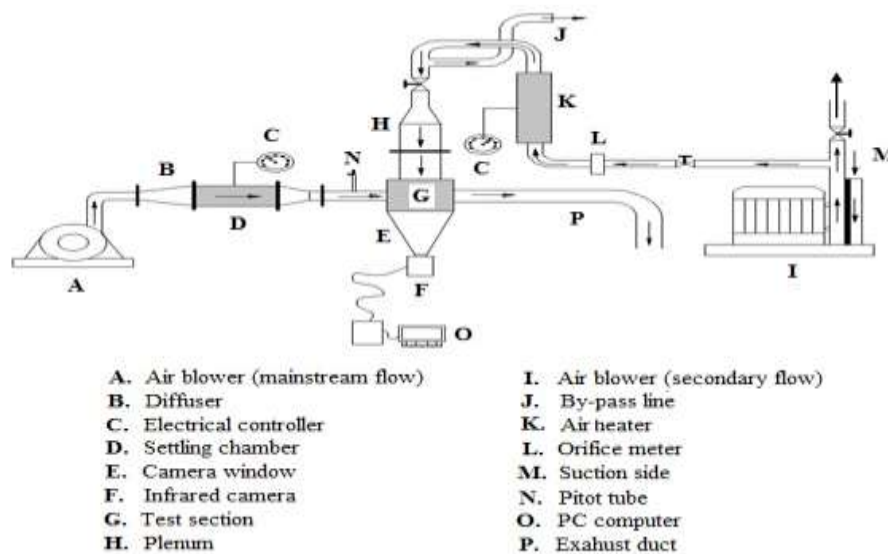
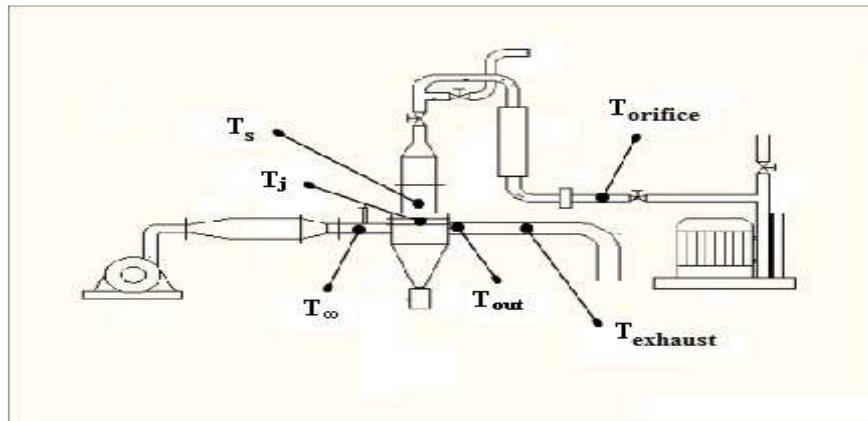


Figure (1): Experimental Test Rig set-up

The mainstream flow is fixed at ($V_{\infty} = 20$ m/s) and ($T_{\infty} = 40$ °C), and the secondary flow is at ($T_s = 100$ °C) with varied mass flow rate according to the required Reynolds number. The flow is turbulent, with Re_j as 5000, 75000, 10000, 12000, and 15000 for inline array and 4200, 6250, 8350, 10000 and 12350 for staggered array that gave same equivalent mass flow rate per unit frontal surface area (G) for both arrays of values (0.95, 1.42, 1.89, 2.27, 2.85). Thermocouples type K are located at

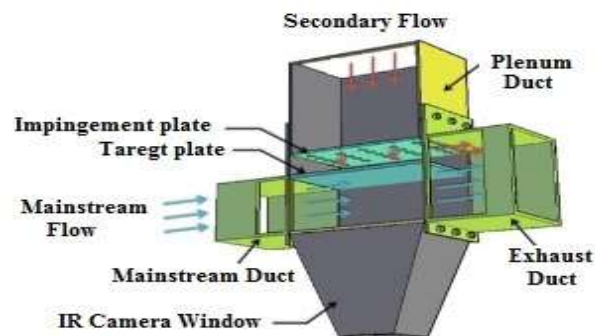
the inlet and exit for the main flow, and the exit of secondary flow temperature as shown in Figure (2).



Figure(2): Show the thermocouple locations in the test rig

The secondary flow rate was measured by using 38 mm diameter orifice plate. The orifice plate is made according to BS1042 [15]. The mainstream velocity was measured by using standard ellipsoidal nosed Pitot- static tube with curved junction (N.P.L Standard). The correction to the reading of the tube was determined according to Ref. [16]. An electrical controller (Variac) is used to control the power supplied to the heaters, therefore maintained the air flow temperature.

The secondary flow passes through the plenum duct and impacts the inner surface of the test plate, while the mainstream flow works as a resistive film on the outer surface of the target plate. Figure (3) shows the schematic diagram of test section. The accuracy of the measurement is estimated according to the methodology of [17], the uncertainties of cooling effectiveness, average Nusselt number and discharge coefficient are set up $\pm 2.56\%$, $\pm 7.79\%$ and $\pm 2.54\%$, respectively.



Figure(3): Schematic diagram of test section

The infrared thermograph (IR) camera type (Fluke Ti32) was used to measure the target outer surface temperatures distribution. The field of view and minimum focus

distance (with standard lens are $23^\circ \times 17^\circ$ and 15 cm respectively; the infrared spectral band range is 8.0 to 14 μm (long wave) and accuracy $\pm 2^\circ\text{C}$ or 2 %; a 320x240 pixel detector.

Jet and Effusion Holes Geometry

The structural form of the impingement test model contains aluminum impingement plate and stainless steel 304 target plate. The impingement plate is perforated and the holes are distributed in inline and staggered arrays. Top view and front section view for both holes arrangements are illustrated in Figs. (4), (5) and (6). The test plate models length and width are (20 cm) and (10 cm) respectively. The jet dimensions and geometries are presented in table (1).

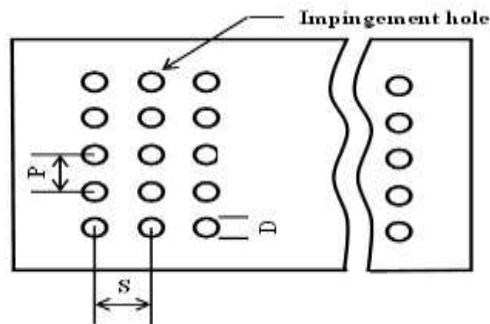


Figure (4): Top view of inline holes

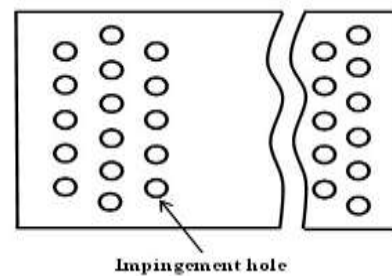


Figure (5): Top view of staggered holes

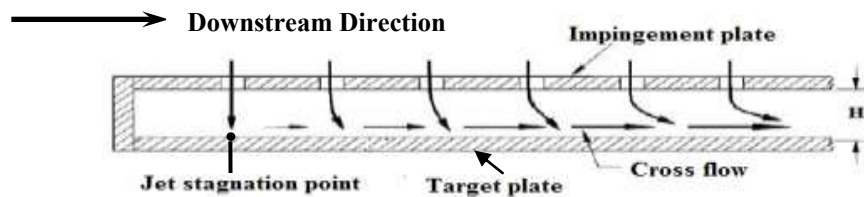


Figure (6): Front view section of the test model

Table (1) Jet holes dimensions geometries

Geometry	Inline array	Staggered array
D (mm)	4	4
Angle of the hole	90°	90°
S/D	4	4
P/D	4	4
H/D	1.5, 2, 3	1.5, 2, 3
No. of the holes	55	66
No. of the columns	11	12
No. of the rows	5	5 - 6
G (kg/s.m^2)	0.95 - 1.42 - 1.89 - 2.27 - 2.85	
Re_j	5000, 7500, 10000, 12500, 15000	4200, 6250, 8350, 10000, 12350
L/D	1	1
Z (mm)	3.5	3.5
A (m^2)	0.02	0.02

Data processing:

The measured physical properties are the entry temperature of the plenum chamber (T_{in}), the mainstream flow (T_{∞}), the exit jet temperature (T_j), the exit secondary flow temperature (T_{out}), target plate thermal conductivity (K), mass flow rate of the secondary flow (\dot{m}) and the target plate outer wall temperature distribution (Tw_o). The principles of the present heat transfer logic calculation are assumed that the energy generated travels into the fluid in a one-dimensional pathway normal to the surface with a uniform heat flux, the internal heat loss by radiation is very small and can be neglected and heat loss from the impingement jet is entirely removed by the mainstream flow. The plenum back side is insulated to minimize the energy

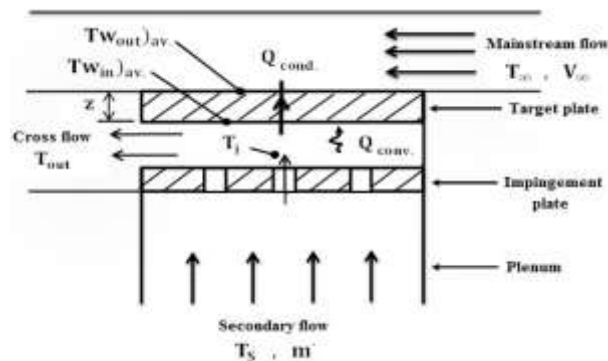


Figure (7): Heat transfer data flow logic sketch

loss to the surrounding and resultant uncertainty in the heat flux into the fluid. Figure (7) summarizes the procedure of the heat transfer data flow logic. The total heat lost from the impinging jets flow by mainstream flow can be calculated as follows:

$$Q_L = \dot{m} C_p \Delta T \quad \dots (1)$$

Where: $\Delta T = (T_j - T_{out})$

T_{out} : Represents the outlet secondary flow temperature (cross flow exit temperature). Since the test section is insulated completely, thus the heat lost removed from the target test plate by the mainstream flow in convection is equal to the heat flux through the wall by conduction such that:

$$Q_L = Q_{Conv.} = Q_{Cond.}$$

The average heat transfer coefficient (\bar{h}) of the internal target plate inner surface according to convection heat transfer equation is given by:

$$\bar{h} = \frac{Q_L}{A((T_{fluid})_{av.} - (Tw_{in})_{av.})} \quad \dots (2)$$

Where,

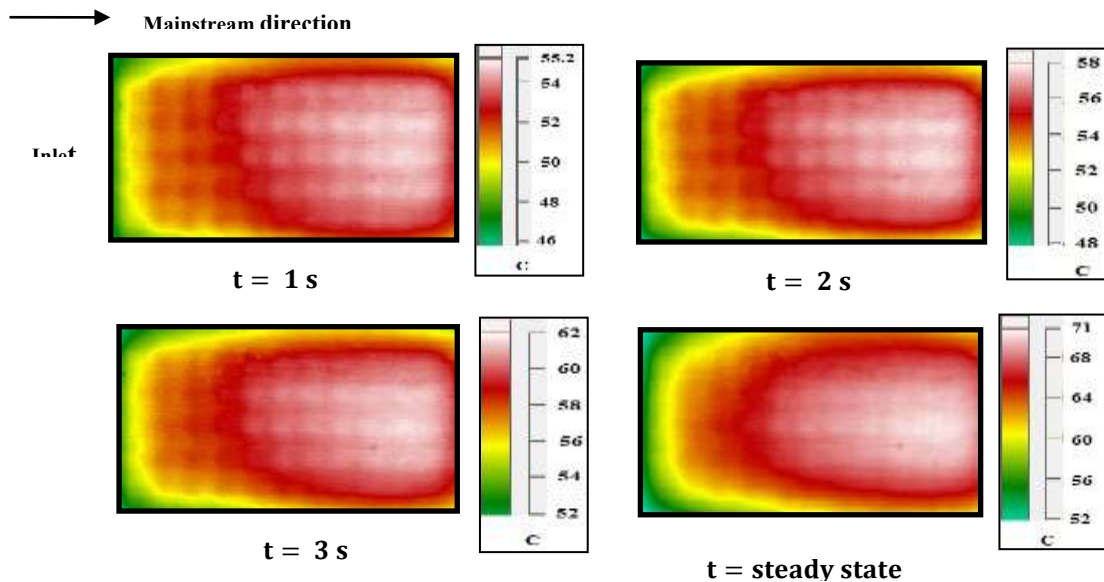
$$(T_{fluid})_{av.} = \frac{T_j + T_{out}}{2}$$

Therefore, the average Nusselt number (\overline{Nu}) obtained is:

$$\overline{Nu} = \frac{\overline{h}D}{K_{air}} \quad \dots (3)$$

The IR Images Validity

Figure (8) shows the IR images for transient heating of the target plate outer surface for inline array. The images show that the contribution impingements jets over the entire area of the target plate, where high temperature is observed at stagnation area. These stagnations regions effect were disappeared with time progress, since the target plate is relatively thick so that the conductivity dominates the heat transfer coefficient induced by the main stream flow on the outer surface of the target plate. This fact gives an indication that the present cooling or heating test techniques are effective in measuring the global average effectiveness and heat transfer rate, therefore the present technique is invalid to measure the local heat transfer coefficient in a steady-state condition.



Figure(8): IR Images on the outer wall of target plate for inline transient case at ($H/D = 1.5$) and ($Re_j = 5000$)

Cooling Effectiveness (η)

Cooling effectiveness is the most relevant parameter for measuring the performance of cooling system. Clearly, if the cooling effectiveness is non-existent, or zero, there is no cooling effect; whereas, if the cooling effectiveness is equal to unity, the liner metal and coolant temperature are the same. These two extreme values of either zero or unity are considered as outer limits for the cooling effectiveness parameter. In general, the cooling effectiveness lies in-between these two limits and characterizes the performance of the cooling system [18]. Cooling effectiveness becomes a major criterion when different cooling techniques are considered. The non-dimensional wall cooling effectiveness is defined as:

$$\eta = \frac{T_{\infty} - T_{w_o}}{T_{\infty} - T_s} \quad \dots (4)$$

Discharge Coefficient Evaluation (c_D)

The flow velocity and the geometrical parameters on the discharge coefficient can be calculated according to [19], the pressure losses at the impingement side are defined by the non-dimensional discharge coefficient as:

$$\Delta P = \frac{m_h^2}{2 A_h^2 C_D^2 \rho}$$

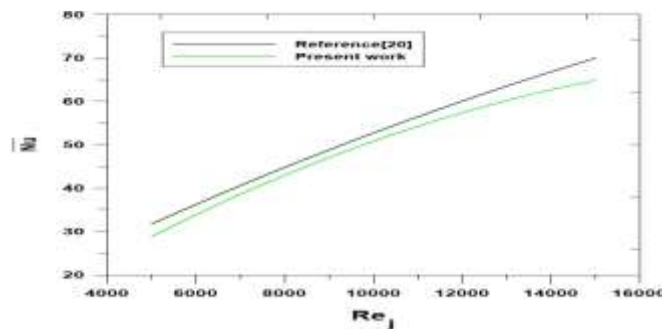
Therefore,

$$C_D = \frac{m_h}{A_h \sqrt{2 \rho \Delta P}} \quad \dots (5)$$

The term (ΔP) represents the difference in the pressure across the impingement wall up to the exhaust which has been measured by a differential manometer.

Experimental Method Verification

To verify the present experimental method of impingement system, the results of average Nusselt number (\overline{Nu}) with (Re_j) are compared with the transient test methods given by [16], the comparison is presented in figure (9). Both tests were conducted for the same holes geometry, inline arrangements, number of holes, and ($H/D = 3$). Same trend of (\overline{Nu}) variation with (Re_j) is observed, and approximately both dictated same level of (\overline{Nu}) values. The minimum and maximum deviation between the experimental and Ref. [20] are (9.6%) and (10.8%), respectively. It is fair to say that the present experimental method is approved to be a reliable.



Figure(9): Comparison of present results with that of [20] (Inline array)

Numerical work

A numerical study is introduced to physically explain the flow characteristics and the phenomena associated with flow field in the jet impingement area. ANSYS FLUENT 14 package is used to perform the numerical simulation of the jet impingement system. Three-dimensional model is introduced, second order upwind is selected for discreteness of the governing equations, and standard ($k - \epsilon$) turbulence model is applied. The air is taken as the working fluid and the flow characteristics are assumed to be steady, Newtonian, incompressible and turbulent. The governing equations, continuity, momentum, and energy for turbulent flow are solved according to [21], [22]. A SOLID WORK PREMIUM 2012 was used to draw

the geometry of the experimental model. Unstructured tetrahedron mesh was used to discretize the computational domain into a finite number of control volumes by using the finite-volume scheme. Figure (10) show the mesh of present model for impingement plate. Structured mesh is ruled out because it is favorable for easy cases and it becomes insufficient and time consumed for complicated geometries [23]. The model was meshed by GAMBIT software.

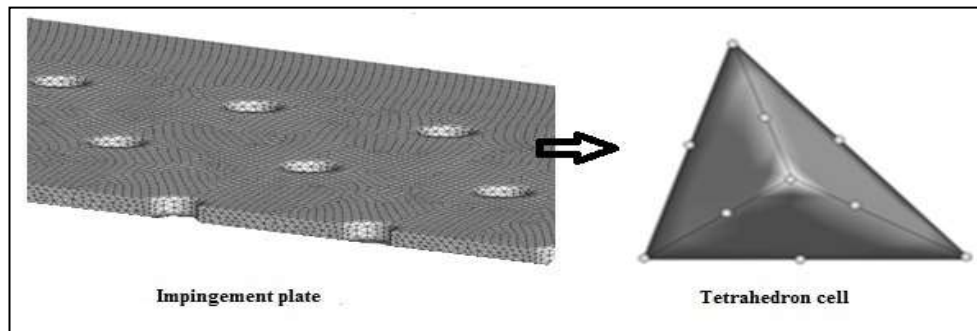


Figure (10): Mesh model

Boundary Conditions:

Both impingement and target plates are regarded as solid boundary surfaces. The volumes of the secondary and mainstream flows are regarded fluid boundary condition. Inlet velocities for both flows are specified. The inlet temperatures for both secondary and mainstream flows are 100°C and 40°C , respectively, while the inlet velocity of mainstream flow is fixed at 20 m/s and secondary flow velocity is adjusted depending on the mass flow rate per unit frontal area (G) required values. Turbulent intensity (TU) for both flows is chosen according to (G) and mainstream velocity values. The hydraulic diameter for both flows depends on the inlet flow geometry. The outlet domain is specified as pressure outlet for both flows, as shown in the figure (11). The pressure is assumed to be atmospheric for both inlet mainstream and outlet secondary and mainstream flows. To reduce the amount of grids and calculation time, symmetric boundary condition is applied on one side of the geometry.

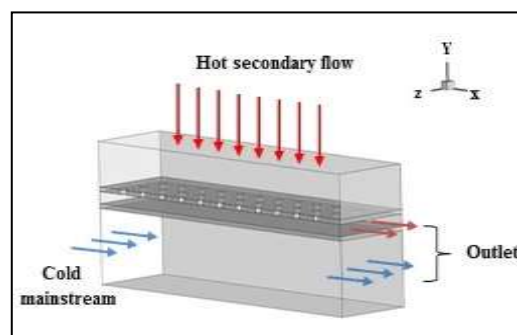
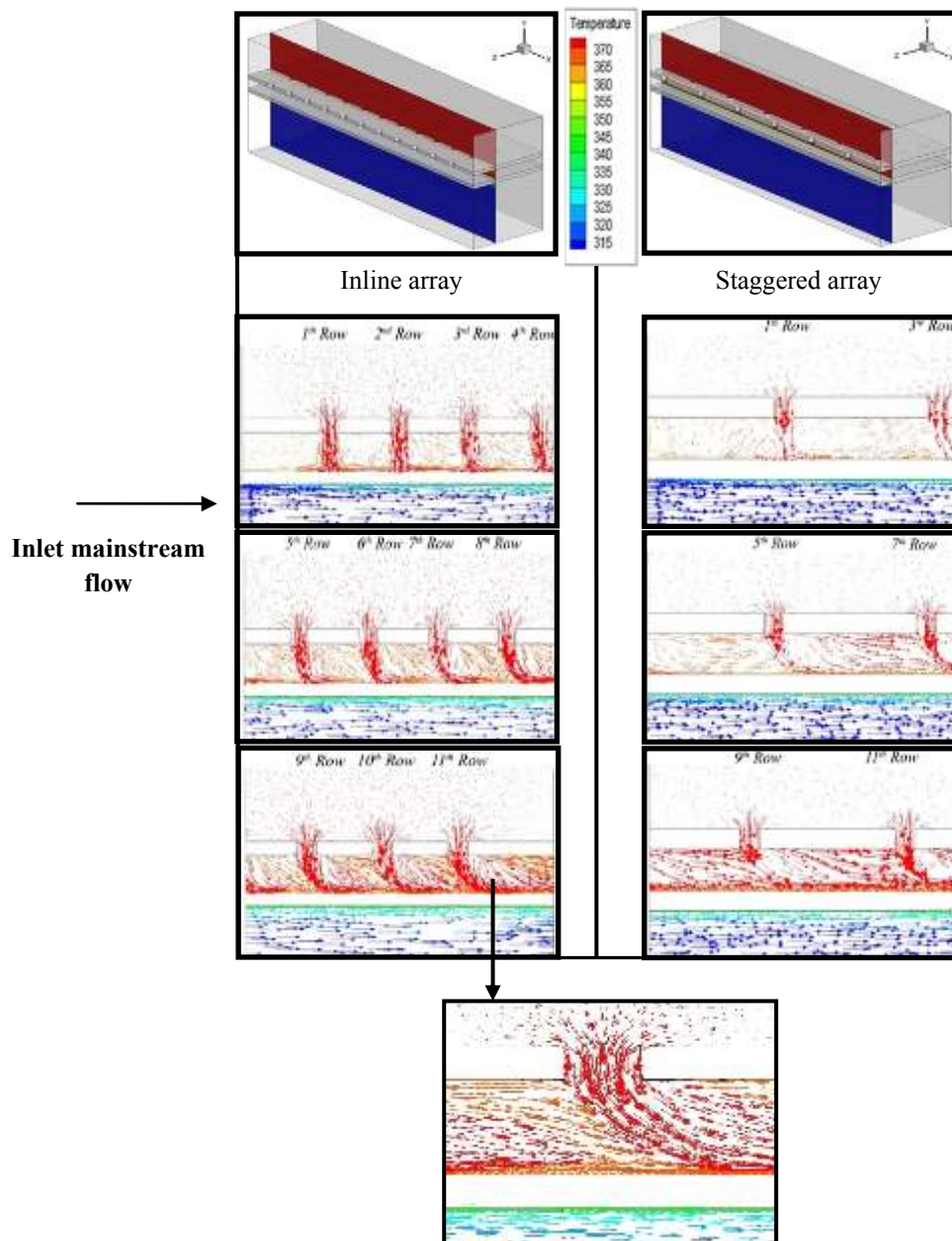


Figure (11): Schematic structure of impingement cooling system

Results and Discussion

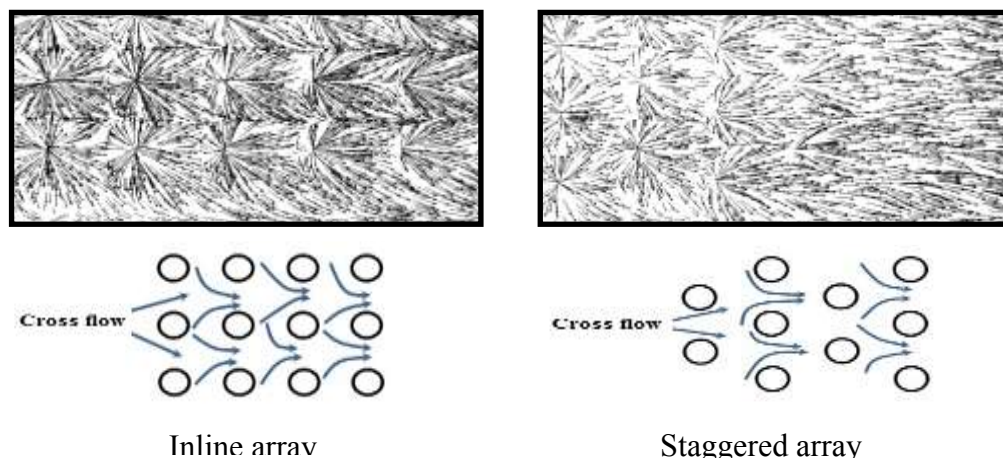
Flow Feature (computational work)

The flow characteristic of impinging jets for inline and staggered arrangements at ($G = 0.95$) and ($H/D = 3$) in x-y plane is shown in the figure (12). For inline array, the result shows the velocity vector within the cooling passage colored by temperature. The impingement jets are deflected away towards the downstream direction due to the effect of cross flow induced by upstream jets. The deflection becomes significant as the flow progresses downstream of the first row. The momentum of the impingement jets is reduced due to the interaction with cross flow, and this affects the rate of heat transfer at stagnation region. This cross flow shows a positive enhancement on heat transfer at the downstream region where high momentum and flow velocity are created due to jet flow accumulation, and this will enhance the cooling effectiveness downstream direction, as shown in figure (8).



Figure(12): Flow vectors colored by temperature in (x-y) plane at ($H/D = 3$) and ($G = 0.95$)

For staggered array, it can be seen that the cross flow velocity has a great influence on the impingement jet, where high deflection is observed at the downstream compared with inline arrangements. Figure (13) shows the velocity vectors in X-Z plane for both inline and staggered arrangements. The results show that the channel flow is induced in inline jet arrangements while in staggered arrangement, these channels are not existed. For inline, the impingements jets are diffused through the channel, resulting low momentum in cross flow that overlaps with the downstream jets while in staggered arrangements, high momentum of cross flow is induced at downstream. This type of flow disturbs the core of impingements jets when it is overlapped, resulting in low local heat transfer at the stagnation region due to jet deflection.



Figure(13): Cross flow characteristics (Computational results)

Experimental work

Wall Cooling Effectiveness

The correct prediction of heat transfer rate needs a profound analysis and understanding of the flow field mechanism. As stated in the literature for impingement system, the optimum jet angle which gives high heat transfer is achieved at 90° , where the maximum momentum of flow is struck on the target plate [6]. Also, it shows that the effects of hole length to diameter (L/D) was not significant for development of impingement jet when L/D is greater than unity [24]; therefore in present work, the study was constrained to $L/D=1$.

The variation of the average wall effectiveness ($\bar{\eta}$) with (Re_j) at different jet height ratios ($H/D=1.5, 2, 3$) are presented in figure (14) for inline arrays. As seen, the wall effectiveness is increased as the Reynolds number increased for all values of H/D . Low values of ($\bar{\eta}$) are observed at ($H/D = 1.5$) with respect to that of ($H/D = 3$). The wall effectiveness is increased by (7.4 %) as (H/D) increased from 1.5 to 3. The narrow spacing between the two plates (jet and target plates) creates a highly constrained cross flow with high momentum and adds more back pressure. The presence of a strong momentum at low H/D tends to disturb the impinging jet pattern at the stagnation region and increases the boundary layer growth on the surface

degrading the heat transfer rates, lowering the wall cooling effectiveness. Generally, best performance is observed at ($H/D = 3$), since the optimum cross flow acceleration is maintained reducing the bad effect at the stagnation region, therefore high recirculation flow between the jets is achieved. These results are in good agreements with results of [25], where high heat transfer coefficient was recorded at $H/D=3$ with independent value of P/D for inline jet arrangement. Figure (15) shows the effect of H/D on the cooling effectiveness for staggered arrays. Slight effect is observed on cooling performance as H/D varied from 1.5 to 3 whereas, only (4 %) increment of cooling effectiveness is obtained.

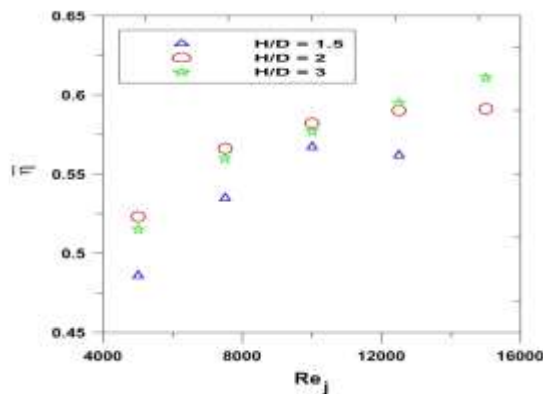


Figure (14): Effect of (H/D) & (Re_j) on ($\bar{\eta}$) (Inline array)

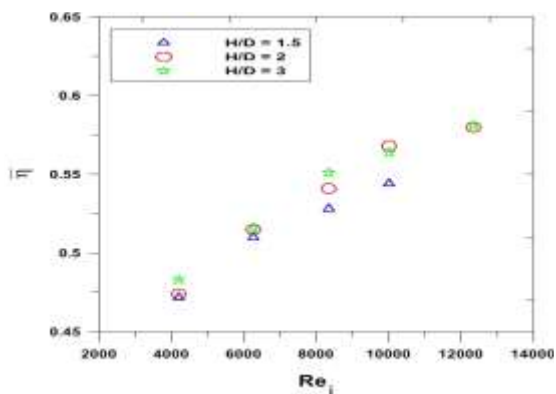
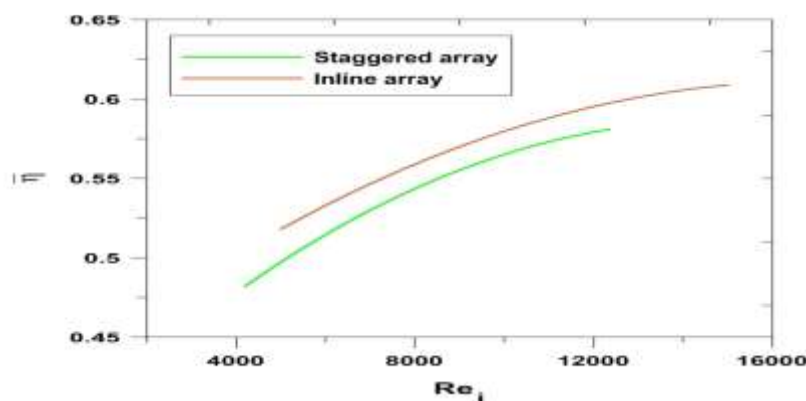


Figure (15): Effect of (H/D) & (Re_j) on ($\bar{\eta}$) (Staggered array)

The average wall cooling effectiveness ($\bar{\eta}$) variation with (Re_j) is presented in figure (16) for ($H/D = 3$). As seen from this figure, the inline array enhanced the cooling effectiveness over that of the staggered array by (10.3 %). As stated before, the cross flow created by the jets didn't disturb the next jet that stands in its pathway for inline arrangement while in staggered configuration, the cross flow disturbed the downstream jets, as shown in the figure (13), therefore the impingement jets of staggered array are not active compared with the inline jets array. The variation of average cooling effectiveness (η_{sa}) along the flow direction for both arrays is presented in figures (17 to 20). For inline arrangement, the cooling effectiveness is increased along the flow direction up to downstream distance of $X/D=30$. Optimum cooling is achieved at $X/D=40$, and slight drop is observed in the region of $X/D>40$. For staggered array, the maximum cooling is achieved at $X/D=25$, and the performance is slightly decayed at $X/D>25$. The reasons are attributed to highly interaction and effect of cross flow on impingement jets induced along the cooling passage.



Figure(16): ($\bar{\eta}$) verses (Re_j) for ($H/D=3$)

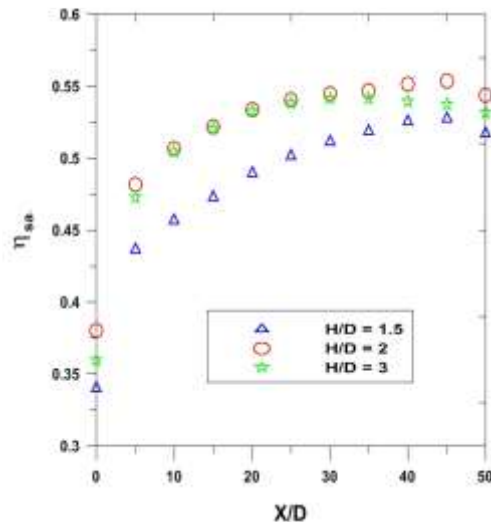


Figure (17): Distribution of (η_{sa}) at ($Re = 5000$) (Inline array)

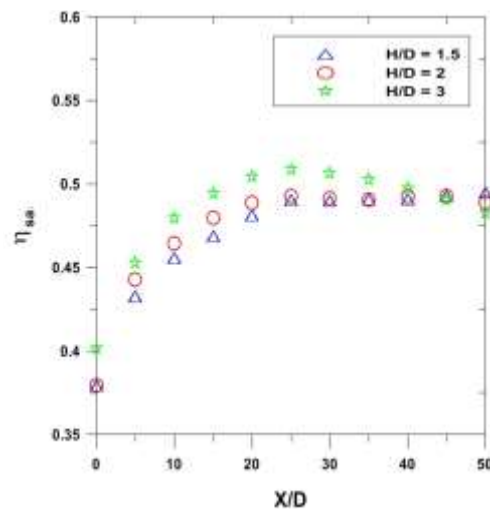


Figure (18): Distribution of (η_{sa}) at ($Re=4200$) (Staggered array)

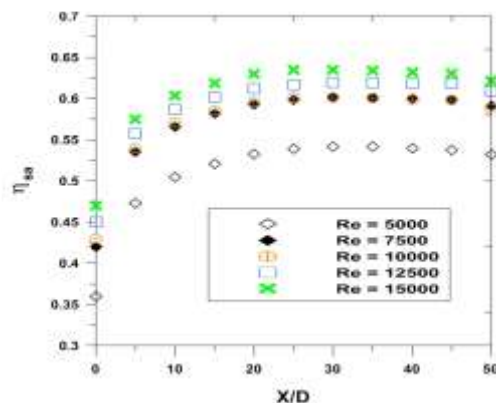


Figure (19): Distribution of (η_{sa}) at ($H/D = 3$) (Inline array)

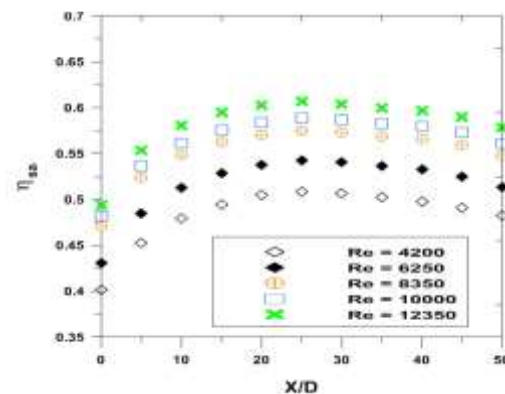


Figure (20): Distribution of (η_{sa}) at ($H/D = 3$) (Staggered array)

Heat Transfer Correlations

The data of cooling performance are presented in terms of Nusselts and Reynolds number in figures (21) and (22). For all (H/D) values, (\overline{Nu}) values are increased with increasing of (Re_j) and maximum heat transfer was obtained at ($H/D = 3$), for both jets arrangement. The average Nusselts number of the present tests results can be correlated using the conventional non-dimensional approach that considering the above parameter as follows:

$$(\overline{Nu} = C Re_j^n (H/D)^m pr^v)$$

Where, C, n, m and v are constants determined by experiments.

The experimental results were gathered, and the least square mathematical technique was implemented to obtain the following correlation for both inline and staggered arrangement.

Inline array:

$$\overline{Nu} = 0.054 Re_j^{0.742} (H/D)^{0.089} Pr^{0.33} \quad \dots \dots \dots (6)$$

Staggered array:

$$\overline{Nu} = 0.069 Re_j^{0.714} (H/D)^{0.04} Pr^{0.33} \quad \dots \dots \dots (7)$$

Figures (23) and (24) present the comparison between the calculated (\overline{Nu}) from experimental data and the correlated (\overline{Nu}), respectively.

The maximum deviation between the experimental (\overline{Nu}) and correlated (\overline{Nu}) for inline array is (6.3%), in the range of ($Re_j = 5000$ to 15000) while for staggered array, the maximum deviation was (5.27%) for the range of ($Re_j = 4200$ to 12350).

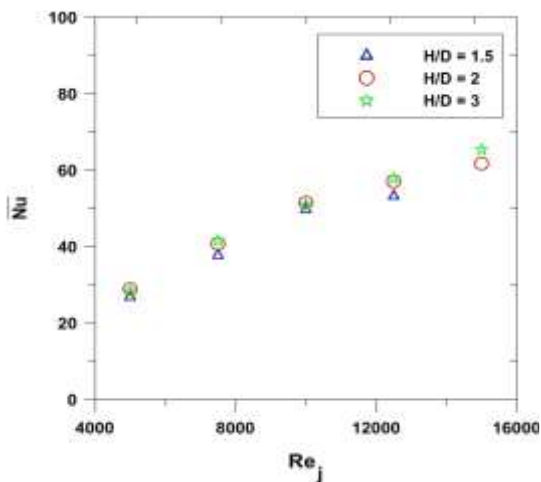


Figure (21): Effect of (H/D) & (Re_j) on (\overline{Nu}) (Inline array)

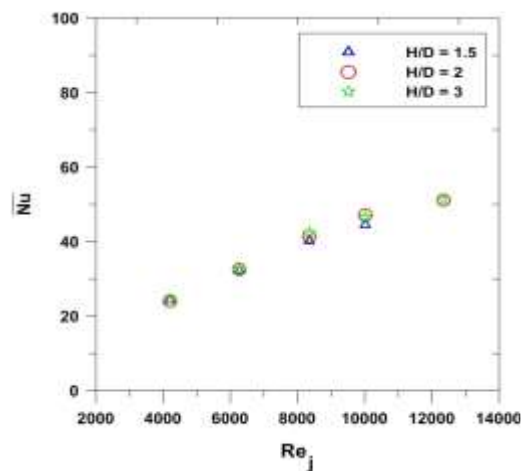


Figure (22): Effect of (H/D) & (Re_j) on (\overline{Nu}) (Staggered array)

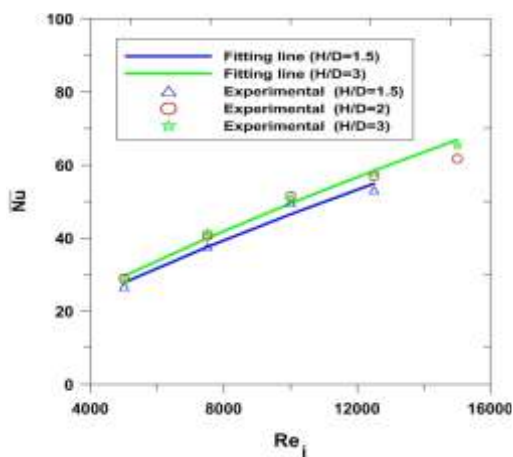


Figure (23): Empirical correlation for (\overline{Nu}) (Inline array)

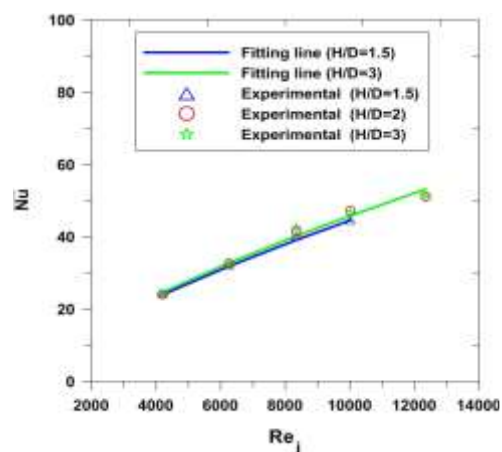


Figure (24): Empirical correlation for (\overline{Nu}) (Staggered array)

Pressure Losses and Discharge Coefficient

The pressure loss is expressed in term of discharge coefficient (C_D), since the pressure drop is a combination of flow contraction in the impingement jet plate and the shear force induced due to friction take places within the cooling passage. Figures (25) and (26) show the influence of (H/D) on the discharge coefficient (C_D) for both inline and staggered arrays. The result shows a significant influence of H/D on the discharge coefficient or pressure drop for both inline and staggered array. For inline array, (C_D) is increased as H/D increased indicating a lower pressure drop as (H/D) increased for the same Reynolds number or jets velocity. In low jet distance (H/D), the cross flow passage is narrowed, therefore the flow shear effect is increased leading to low (C_D) values. The same are observed for staggered arrangement as H/D varied from 1.5 to 3.

For $H/D \geq 2$, the result depicts a slight increment in discharge coefficient with increasing Re up to $Re = 10000$, since the cross flow and shear force are increased. These results indicate that best jets flow characteristic can be achieved when $Re > 10000$. This claim is complied with the results of ($H/D = 2$), since the discharge coefficient declined after $Re \geq 12000$ where the high cross flow velocity is exist. High frictional shear forces within the passage are dominated the pressure loss. At ($H/D = 1.5$), the discharge coefficient is almost constant. The inline arrays give high discharge coefficient and low pressure loss. This is attributed to high cross flow interaction with jets. This interaction plays an important role of depleting the cross flow momentum resulting of high pressure drop.

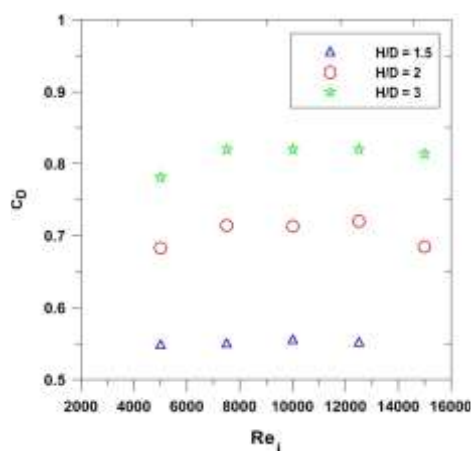


Figure (25): Influence of (H/D) and (Re_j) on (C_D) (Inline array)

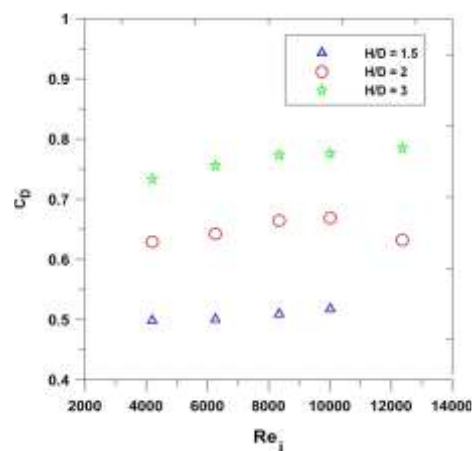


Figure (26): Influence of (H/D) and (Re_j) on (C_D) (Staggered array)

CONCLUSIONS

The heat transfer characteristics and pressure loss have been investigated and the following conclusions can be derived from the present work for impingement cooling system.

- 1- Numerical prediction of the flow field structure for both inline and staggered arrays showed the effect of cross flow on the shift jet stagnation point, especially at mid and end distance test plate. Thus, the cross flow has major effects on cooling

performance, and the effect of cross flow on the staggered array is more than inline array.

- 2- The present experimental model is able to predict both the heat transfer coefficient and the wall cooling effectiveness.
- 3- The narrow spacing (H) between the two plates (jet and target plates) creates a highly constrained cross flow with high momentum and adds more back pressure, therefore best performance is observed at ($H/D = 3$).
- 4- The inline arrays enhanced the wall cooling effectiveness by (10.3%) at ($G=0.95$), at ($H/D = 3$).
- 5- Empirical correlations for both cases are introduced for the area-averaged Nusselt number. The maximum deviation between the experimental and correlated (\overline{Nu}) values are (6.3%) and (5.27%) for inline and staggered arrays, respectively.
- 6- Both jet spacing and Reynolds number have an evident effect on the discharge coefficient. For both cases, low (C_D) values are obtained at jet spacing 1.5 and high (C_D) at jet spacing 3.0.

REFERENCES

- [1].Tawfek A. A., (2002), "Heat transfer studies of the oblique impingement of round jets upon a curved surface", *Int. J. Heat Mass Transfer*, Vol. 38, pp. 467–475.
- [2].Zuckerman N. and Lior N., (2005), "Impingement heat transfer: correlations and numerical modeling", *J. Heat Transfer*, Vol. 127, pp. 544-552.
- [3].San J. Y. and Lai M., (2001), "Optimum jet-to-jet spacing of heat transfer for staggered arrays of impinging air jets", *Int. J. Heat Mass Transfer*, Vol. 44, pp. 3997–4007.
- [4].Changmin S., David G., Peter I. and Geoffrey M., (2001), "Heat transfer and flow characteristics of an engine representative impingement cooling system", *International Gas Turbine Institute, ASME Journal of Turbomachinery*, Vol.123.
- [5].Brevet P., Dejeu C., Dorignac E., Jolly M., and Vullierme J. J., (2002), "Heat transfer to a row of impinging jets in consideration of optimization", *International Journal of Heat and Mass Transfer* 45, pp. 4191-4200.
- [6].Lamyaa A. E., and Deborah A.K., (2005), "Experimental investigation of local heat transfer distribution on smooth and roughened surfaces under an array of angled impinging", *ASME Journal of turbomachinery*, Vol.127, pp. 590-597.
- [7].Uysal U., Chyu M.K., and Cunha F.J., (2006), "Heat transfer on internal surface of a duct subjected to impingement of a jet array with varying hole size and spacing", *ASME Journal of Turbomachinery*, Vol.128, pp. 158-165.
- [8].Eric I. E., (2006), "Jet impingement cooling configuration for gas turbine combustion", Master thesis submitted to the graduate faculty of the Louisiana State University and Agricultural and Mechanical College.
- [9].Lee J. and Lee S., (2000), "The effect of nozzle configuration on stagnation region heat transfer enhancement of axisymmetric jet impingement", *Int. J. Heat Mass Transfer*, Vol. 43, pp. 3497–3509.
- [10].Zuckerman N., and Lior N., (2006), "Jet impinging heat transfer: physics, correlation, and numerical modeling", *Advances in Heat Transfer*, Vol. 39, pp. 565-630.
- [11].Perapong M. W., and Chayut N., (2013), "Influence of nozzle arrangement on flow and heat transfer characteristics of array of circular impinging jets", *Songklanakarin Journal of Science and Technology*, 35(2), pp. 203 -212.

- [12].Yoshisaburo Y., Yoshiyasu I., Makoto Y., and Shinji H., (2012), "Effect of injection parameters on jet array impingement heat transfer", International Journal of Gas Turbine, Propulsion and Power Systems, Vol. 4, No.1.
- [13].alal M., Sabah A., and Adnan A., (2009) "Impingement cooling characteristics of a cube in cross flow", Eng. & Tech. Journal, Vol. 27, No. 4, University of technology, Iraq.
- [14].Assim H., Amer M., and Salah H., (2015) "Heat transfer and flow performance of impingement and impingement/effusion cooling systems", Eng. & Tech. Journal, Vol. 33, Part (A), No. 6, University of technology, Iraq.
- [15].BS1042 Standard, "Method of measurement of fluid flow in closed conduits", Part 1, Section 1.1, 1980.
- [16].BS1042 Standard, "Method for the measurement of fluid flow in pipes", Part 2A, 1974.
- [17].Kline S. J., and McClintock F. A., (1953), "Describing uncertainties in single sample experimental", Mechanical Engineering, Vol. 75, pp. 3-8.
- [18].Frank J. C., (2006), "Heat transfer analysis", The Gas Turbine Handbook, 4.4, pp. (389-410).
- [19].Amer. M. H., "Compact heat exchanger design using enhanced effective heat transfer", Ph.D. thesis submitted to the Department of Fuel and Energy, University of Leeds, 1991.
- [20].Andrew S., Shichuan O., and Urmila G., (2012) "Experimental study of an impingement cooling jet array using an infrared thermography technique", Journal of thermophysics and heat transfer, Vol.26, No. 4, pp. 590-597.
- [21].Versteeg H. K. and Malalasekera W., (1996), "An introduction to computational fluid dynamics the finite volume method", Longman Group, London.
- [22].Roy D. N., (1987), "Applied fluid mechanics", Affiliated East-West Private LTD, New Delhi.
- [23]. "Fluent 14 use: guide, programing and tutorial guide", Fluent, Version 14, Ansys Inc., 2010.
- [24].Andrew G. E., Durance J., Hussain C. I. and Ojobor S. N., (1987), "Full coverage impingement heat transfer: influence of the number of holes", ASME, Journal of Turbomachinery, Vol.109, pp. (557-563).
- [225].Brevet P., Dejeu C., Dorignac E., Jolly M., and Vullierme J. J., (2002) "Heat transfer to a row of impinging jets in consideration of optimization", International journal of heat and mass transfer 45, pp.4191-4200.